Climate change threatens olive oil production in the Levant

David Kaniewski, Nick Marriner, Christophe Morhange, Carla Khater, Jean-Frédéric Terral, Guillaume Besnard, Thierry Otto, Frédéric Luce, Quentin Couillebault, Labrini Tsitsou, et al.

This is a postprint version, the definitive version of this paper is :

Kaniewski, D., Marriner, N., Morhange, C., Khater, C., Terral, J.-F., Besnard, G., Otto, T., Luce, F., Couillebault, Q., Tsitsou, L., Pourkerman, M., & Cheddadi, R. (2023). Climate change threatens olive oil production in the Levant. Nature Plants, 1-9. https://doi.org/10.1038/s41477-022-01339-z

Climate change threatens olive oil production in the Levant

David Kaniewski[1,2]†, Nick Marriner[3]†, Christophe Morhange[4,5], Carla Khater[6], Jean-Frédéric Terral[7], Guillaume Besnard[8], Thierry Otto[9], Frédéric Luce[9], Quentin Couillebault[1,10], Labrini Tsitsou[4], Majid Pourkerman[11], Rachid Cheddadi[7]†

[1]TRACES, UMR 5608 CNRS, Université Toulouse Jean Jaurès, Maison de la Recherche, 5 allées A. Machado 31058 Toulouse Cedex 9, France
[2]Département de Biologie et Géosciences, Université Paul Sabatier - Toulouse 3, Toulouse cedex 9, France
[3]CNRS, ThéMA, Université de Franche-Comté, UMR 6049, MSHE Ledoux, 32 rue Mégevand, 25030 Besançon Cedex, France
[4]Aix Marseille Université, CNRS, IRD, INRA, Collège de France, CEREGE, Aix-en-Provence, France
[5]EPHE-Section des Sciences Historiques et Philologiques, AOROC, UMR 8546 - Archéologie et Philologie d'Orient et d'Occident, CNRS/PSL, École Normale Supérieure, 45 rue d'Ulm, 75230 Paris Cedex 5, France
[6]Center for Remote Sensing, National Council for Scientific Research - Lebanon, BP 11-8281, Bir Hassan, Beirut, Lebanon
[7]Université Montpellier II, CNRS-UM-IRD, ISEM, France
[8]Laboratoire Évolution & Diversité Biologique (EDB UMR 5174), Université de Toulouse, CNRS, UPS, IRD, Toulouse, France
[9]Laboratoire Ecologie Fonctionnelle et Environnement, Université de Toulouse, CNRS, INP, UPS Toulouse cedex 9, France
[10]Aix Marseille Université, CNRS, CCJ, Centre Camille Jullian, Aix en Provence, France
[11]Iranian National Institute for Oceanography and Atmospheric Sciences (INIOAS), 3 Etemad Zadeh St., Fatemi Ave., 14155-4781 Tehran, Iran

Corresponding author: David Kaniewski (ORCID https://orcid.org/0000-0001-6569-3184)

Email: david.kaniewski@univ-tlse3.fr

† These authors contributed equally to this work

The olive tree (*Olea europaea* L.) is one of the best-adapted species to Mediterranean-type climate[1-8]. Nonetheless, the Mediterranean Basin is deemed to be a climate change "hotspot" by the IPCC[9,10] because future model projections suggest considerable warming and drying[11,12]. Within this context, new environmental challenges will arise in the coming decades, which will both weaken and threaten olive-growing areas, leading to a loss of productivity and changes in fruit and oil quality[13-15]. Olive growing, a core of the Mediterranean economy, might soon be under stress. To probe the link between climate and olive trees, we here report 5400 years of olive-tree dynamics from the ancient city of Tyre, Lebanon. We show that optimal fruiting scales closely with temperature. Present-day and palaeo-data define an optimal annual average of 16.9±0.3°C for olive flowering, that has existed at least since the Neolithic. According to our projections, during the second half of the 21st century, temperature increases in Lebanon will have detrimental consequences on olive-tree growth and olive-oil production, especially in the country's southern regions that will become too hot for optimal flowering and fruiting. These data provide a template to understand present and future thresholds of olive production under climate change.

Olive is one of the oldest cultivated species in the world, an iconic tree, a symbol of identity and a marker of the Mediterranean area, of its bioclimate and, above all, a central staple of its economy[1-8]. The tree was probably domesticated in the Levant, the original centre of three E1 haplotypes which are common (>85%) in most current cultivars[16]. Moreover, the comparison of the geographical pattern of plastid diversity between wild and cultivated olives further indicates that the cradle of domestication is located in the northern Levant, followed by diffusion across the Mediterranean Basin, in tandem with the expansion Mediterranean cultures and human exchanges[6,17]. Nowadays, there are >2000 cultivars in the Mediterranean Basin[18] and their geography overlaps with their wild relatives[7,19-21].

Olives feature among the main Mediterranean orchard crops and are valued primarily as a source of oil for eating and cooking[22]. The earliest evidence of olive-oil extraction, based on oleaster, is dated to 6700-6500 ^{14}C BP and was unearthed south of Haifa at the submerged Neolithic sites of Kfar Samir, Kfar Galim and Tel Hreiz[23-25]. Olive-oil production, trade and economy strongly increased during the Bronze Age (5300-3200 BP), reaching an acme from the Persian period to the Byzantine era[7]. Nowadays, the olive oil economy is mainly centered on the western Mediterranean and constitutes a 13.03-billion-USD industry (2019)[26], with a

market led by Spain, Italy, Tunisia, Greece and Turkey. For instance, in 2019-2020, these five countries produced 2,436,000 tons of olive oil, which represents ~75% of the global production[26].

At a Mediterranean scale, the effects of climate change[9-12] on olive-oil production and economy must be considered as a serious threat to present and future production[13-15]. Rising temperatures and precipitation shortages have already affected olive production in recent decades and projections of increasing Growing Season Temperature will enhance future water demands, potentially leading to a 45 % decline in the main production regions[27]. A number of recent studies have highlighted the detrimental effects of drought stress, rising temperatures and heat waves on olive yields[28-30]. While Lebanon only accounted for 19,000 tons of olive-oil production in 2019 (<1% of world production), with exports totaling USD 22.55 million[31], olive growth is directly threatened by climate change[32]. In Lebanon, a total of 563 km^2 is occupied by olive trees, representing 5.4% of the territory and 8.5 % of total agricultural land[31] (Extended Data Fig. 1). Lebanese trees are on average 150 years old, with a density of ~207 trees per hectare, and are mainly rainfed[31]. The country's main varieties are Souri and Baladi, but other cultivars such as Shami, Ayrouni, Smoukmouki and Shetawi are also used for olive-oil production[33].

While the impact of climate change in Lebanon has long solicited concern, particularly with regards to water resources[34-37], the potential effect on the country's olive groves is unknown, generating economic insecurity in one of Lebanon's key agricultural sectors, ranking second after fruit production. The olive industry supports 170,000 farmers. To probe the potential impact of climate change on olive orchards, we here reconstruct past, present and future trends to quantify the evolution of olive-growing in Lebanon.

Using pollen analysis and pollen-derived climate models, we reconstructed 5400 years of olive-tree dynamics and climate variations (from 7720±70 to 2350±60 BP; Fig. 1) from a sediment core (T-XXI), sampled close to the Al-Bass necropolis in the city of Tyre, located 83 km south of Beirut (Extended Data Fig. 2). The chronology of the 390-cm core is based on thirteen ^{14}C dates (Extended Data Fig. 3). The city is documented to have been founded in the Bronze Age[38], during the third millennium BC[39], but olive is recorded as early as 7700±70 BP (Neolithic), with high influx values at the end of the Neolithic and during the Chalcolithic (Fig. 1). These early records of olive at Tyre can only derive from the wild variety (oleaster) and result from a natural occurrence and expansion before any human domestication. Olive pollen has also been recorded ~8000-7500 BP in the Bekaa Valley (Aammiq, Chamsine and Al Jourd

wetlands)[40-42], suggesting that olive trees were already widely present in Lebanon before their domestication. Since the Bronze Age and the domestication of olive trees, significant pollen influx values have been recorded, suggesting a more marked occurrence and probably a more sustained pollen production/flowering (Fig. 1). A downturn in olive growing began during the final part of the Bronze Age and continued during the Phoenician and Persian periods when olive groves were less important (presence and pollen production).

To test the role of climate in olive-pollen production/flowering (Fig. 1), we defined a temperature and precipitation preferendum (Fig. 2a-b) based on 325 present olive-growing areas rimming the Mediterranean Basin (Extended Data Fig. 4). We reconstructed an optimal annual mean temperature (T_{mean}) for olive orchards of 16.9±0.3°C with a 25th percentile of 15.7°C and a 75th percentile of 18.3°C (Fig. 2a). These values are consistent with the range of 15 to 25°C defined as the optimum T_{mean} required for the growth and development of olive fruits[43]. They are also consistent with the T_{mean} of 14.5°C which corresponds to the lower limit for olive growth[43]. When the distribution of olive pollen at Tyre is plotted against the reconstructed T_{mean} and contrasted with the present-day optimum, the high values fall between the percentiles and the highest scores are clustered around the annual modern optimum (Fig. 2a). Because olive trees are sensitive to seasonality[14,27], we used the distribution of olive pollen at Tyre plotted against the reconstructed temperatures for January (Extended Data Fig. 5a), February-March (Extended Data Fig. 5b), spring (Extended Data Fig. 6a) and summer (Extended Data Fig. 6b). We defined the present-day optimum for each month/season based on the 325 present-day olive-growing areas. We found optimal values of 8.7±0.3°C (January), 10.5±0.3°C (February-March), 15.6±0.3°C (spring) and 23.8±0.3°C (summer). In each case, the high and maximum values of pollen production/flowering from the Neolithic to the Persian period are within the optimum temperature range defined by the 325 present-day stations. This suggests that past and present olive yields are mediated by the same climatic parameters and the same temperature optima. We also reconstructed the minimum (T_{min}) and maximum (T_{max}) temperatures for the coldest month (January) and the hottest season (summer) to test if frost or excessive heat may have affected the olive trees (Extended Data Fig. 7a-b). Olive tissues are damaged at -5/-7°C when the leaves, shoots, twigs, and stems freeze, and at $\geq$30°C when the enzymes involved in photosynthesis are denatured and the photosynthesis rate decreases, negatively affecting fruit formation[43]. We reconstructed an average January T_{min} of 4.2±0.6°C (Extended Data Fig. 7a), with a lowest value of 2.5°C (2950 to 2850±65 BP), and an average summer T_{max} of 28.9±0.3°C (Extended Data Fig. 7b), with a highest value of 29.9°C (7670 to

7650±70 BP). Olive trees at Tyre were not directly damaged by frost or by heat waves, suggesting that trees may have easily persisted from the Neolithic to the Persian period. The main dynamic recorded therefore correspond to temperature-based variations in pollen production/flowering, which in turn mediated the quantity of olive fruits produced.

Focusing on precipitation, we defined an optimal annual average of 575±22 mm with a 25th percentile of 447 mm and a 75th percentile of 672 mm based on the 325 present-day olive-growing areas (Fig. 2b). The value of 575±22 mm may seem low compared to the annual rainfall amount of 700 to 850 mm that is required for olive groves[43], but the seasonal precipitation distribution is more important than the total annual amount[44,45]. Two seasons are particularly significant, spring when the olive trees produce new shoots, buds and flowers, and summer for fruiting. We calculated seasonal values of 128±5 mm (full range: 101-140 mm) for spring and 46±5 mm (full range: 17-57 mm) for summer. The distribution of olive pollen at Tyre was then plotted against reconstructed precipitation and contrasted with the present-day optimum (Fig. 2b and Extended Data Fig. 8a-b). It appears that the distribution of olive pollen is less clear when applied to precipitation (Fig. 2b). Several influx values, both low and high, are clustered around the present-day optimum. Nevertheless, the majority of the data points (Fig. 2b and Extended Data Fig. 8a-b) fall between the modern optimum and the 25th percentiles, suggesting a coherency between the past and the present. The olive tree seems to have a much wider ecological range in terms of precipitation than temperature, but is not recorded in environments that are too wet or too dry. Below 450 mm of annual rainfall (Fig. 2b), <100 mm in spring (Extended Data Fig. 8a) and <17 mm in summer (Extended Data Fig. 8b), the olive tree does not have an optimal fruiting cycle and olive production is negatively affected by drought.

Olive influx and reconstructed T_{mean} were averaged by cultural period using boxplots (Fig. 3) to explore the maximum pollen production/flowering. Higher values of pollen production/flowering were recorded during the Chalcolithic and the Bronze Age, two periods defined by temperatures that include the present-day annual optimum. The Neolithic appears to have been too warm for an optimal pollen production, whereas, by contrast, the Phoenician and Persian periods were probably too cool.

Based on Lebanese olive-oil data (period 1991-2020)[26], we compared the evolution of production according to the temperatures in North Lebanon, the country's main production region (41% of olive oil production; Extended Data Fig. 1). We defined an optimum of 16.8°C for olive-oil production with a tolerance of ±0.6°C (Extended Data Fig. 9a), close to the

16.9±0.3°C outlined by the 325 present-day olive-growing areas in the Mediterranean Basin. We then applied the same procedure to the olive influx at Tyre, with the reconstructed T_{mean}, and compared and contrasted the results with present-day olive oil production (Extended Data Fig. 9b). The two Gaussian curves, illustrating the optimum and the tolerance zones for each dataset, fit closely, suggesting that pollen influx (pollen production/flowering) is correlated with olive-oil production and may serve as proxy to estimate past trends in olive-oil production.

Olive trees present an adaptive mechanism to respond to drought stress and avoid serious oxidative damage[46]. A major process is the accumulation of phenolic and lipophilic compounds directly activated by water shortages[47,48]. If drought stress occurs between early ripening and the harvesting stages of olives (October-November)[49], phenolic and lipophilic compounds build-up in the fruit. The accumulation of these compounds increases the nutritional value of olives, with phenolic and lipophilic compounds transferred to oils, yielding different but refined tastes[50,51]. To investigate if drought stress may have influenced the gustatory attributes of olive oil at Tyre, we first calculated an optimal value for October-November (ripening and harvesting stages of olives), based on the 325 present-day olive-growing areas. An average value of 135±5 mm (full range: 105-165 mm) was determined (Extended Data Fig. 10). At Tyre, the average for October-November (from the Neolithic to the Persian period) was 103±6 mm, just under the lower threshold of 105 mm (Extended Data Fig. 10). Drought stress seems to have affected the olive trees, causing an accumulation of phenolic and lipophilic compounds in fruits, and later, in oils. We hypothesize that the olive oil from Tyre, although not necessarily produced in high quantities, would have been sought after for its high nutritional value and refined taste.

We performed climate projections for the year 2100 in Lebanon, calculating the rising rate in temperature for each region (Fig. 4a-e), using the period 1961-1990 as a baseline (Fig. 4). The temperature anomalies for 2100 vary regionally from 2.2±0.45°C to 2.3±0.45°C, consistent with the 2.2°C projected by the CMIP6 (scenario SSP1-2.6; relative to 1961-1990) for the Mediterranean Basin[52]. When the annual optimum for olive growth (16.9±0.3°C) is compared and contrasted with the projected evolution of temperatures in Lebanon, the data suggest that South Lebanon (Fig. 4c) and Nabatieh (Fig. 4d) will become unsuitable for olive-oil production. Mount Lebanon (Fig. 4b) and North Lebanon (Fig. 4a) will reach the upper threshold (18.3°C) while the Bekaa (Fig. 4e) will remain below the lower threshold (15.7°C) for an optimal production. The country's olive-oil economy will therefore be strongly affected by climate change.

The occurrence (pollen production/flowering) of olive trees (wild and cultivated) in Lebanon seems to have been controlled by climate parameters since the Neolithic (Fig. 1) even if human societies, since the Late Chalcolithic and Early Bronze Age, have domesticated the tree for economic reasons. The main limiting factor for an optimal yield is temperature (both annual and seasonal). The olive tree appears to be very sensitive to temperature variations for flowering and fruiting (Fig. 2a). The annual optimum value of 16.9±0.3°C (full range: 15.7-18.3°C), defined using present-day olive groves, also corresponds to the optimum since the Neolithic (Fig. 3). The lower and upper thresholds of 15.7°C and 18.3°C are clear limits between which olive trees had a high pollen production from the Neolithic to the Persian period. When present-day olive-oil production in Lebanon is contrasted with past olive-pollen production at Tyre, the same trend emerges, with an optimum centered on 16.8°C and tolerance zones of ±0.6°C (Extended Data Fig. 9b), close to the optimum value of 16.9±0.3°C, suggesting that efficient olive-oil production is also linked to temperature. Olive trees are also dependent on precipitation, mainly at a seasonal scale. They are especially sensitive to a decrease in rainfall, even if the tolerance zone (full range: 447-672 mm) seems larger compared to temperature (Fig. 2b). Of the two most important seasons (spring and summer), spring seems to be the key period (Extended Data Fig. 8a), when olives produce new flowers which will later develop into fruits. If spring is too dry (or too wet), the olive tree will not have an optimal fruiting cycle and olive production will be negatively affected.

As the olive tree is sensitive to temperature and precipitation, projected climate change in Lebanon (Fig. 4) will have a substantial impact on the olive-oil economy and will directly threaten the country's agricultural industry. The southern territories (South Lebanon and Nabatieh) will become unsuitable for olive oil production without any technology-based adaptations[32] or breeding of new cultivars adapted to drought and increasing temperature[53,54]. The northern regions (North Lebanon and Mount Lebanon) will experience major changes, with a rise in temperatures that could greatly reduce olive yields. The eastern parts of the country will remain unfavorable for efficient olive-oil production. While irrigation can be used to counter increasing water demand resulting from more frequent and more intense drought stresses, it will be increasingly challenging to offset the negative effects of rising temperatures, with wider Mediterranean-scale implications for olive production under climate change.

Methods

Core and chronology. The core T-XXI was drilled in the marshland (33°16'18.21"N, 35°12'56.48"E, 4 m a.s.l.) close to the Al-Bass necropolis in Tyre (Extended Data Fig. 2). The lithology of the core T-XXI is heterogeneous (Extended Data Fig. 3) with a sandy matrix overlain by 390 cm of undisturbed muddy silts rich in bioindicators. The upper layer was not studied because it has been disturbed by anthropogenic activity. The core was sampled every 2 cm. The chronology of the core T-XXI (Extended Data Fig. 3) is based on thirteen ^{14}C dates performed on short-lived terrestrial samples (small leaves and seeds). All the botanical macro-remains were sent to Beta Analytic (Florida). The ^{14}C dates were calibrated to 2σ using Calib Rev 8.0.1 (IntCal20). All the calibrated ages are denoted in BP and BC, consistent with the archaeological/historical data.

Palaeoecological data. Samples from the core T-XXI were prepared for pollen analysis using standard procedures for clay-silt samples[55]. Pollen grains were counted under x400 and x1000 magnification using an Olympus microscope. The mean pollen sum was 351±38 pollen grains, with a minimum of 301 pollen grains. The median value was 344 pollen grains, with a 25th percentile of 319 pollen grains and a 75th percentile of 377 pollen grains. For olive trees, the pollen influx was calculated (Fig. 1). Because the amount of pollen produced by an olive tree is dependent on flowering (small, white flowers arranged in inflorescences of 15-35 flowers)[56], these two notions (pollen production/flowering) were assimilated in this study. The pollen influx (or Pollen Accumulation Rate - PAR) is defined as the number of pollen grains accumulated per unit of sediment surface area and per unit of time (grains cm^{-2} yr^{-1}). The long-term trend was calculated using a polynomial model. As the distinction between the cultivated and non-cultivated varieties of *O. europaea* is palynologically impossible[57] as well as discrimination between different cultivars, the ensemble is collated into a single signal, giving the main trends since the Neolithic. A regular chronological interpolation (20-yr) was applied to the dataset in order to reduce biases linked to chronological gaps, particularly at the bootstrap level. We then transformed the influx scores using a Loess smoothing (with a LOWESS algorithm) and performed a bootstrap to estimate a 95% confidence band based on 1000 random replicates. The Loess curve and the 95% confidence band were used as a proxy for olive pollen influx (Fig. 1).

Statistical analyses. Statistical analyses were performed using Xl-Stat[2019], R software version 3.6.3[58] and the software package PAST 4.08[59].

Pollen-derived climate reconstruction. The pollen-based model used to reconstruct the climate variables (Fig. 1) is fully described in the literature[42,60] and has proven to provide coherent climate reconstructions[61-63]. We assigned fossil pollen taxa to modern plant species for which we have georeferenced distributions archived in a dedicated database. We excluded aquatic plants, helophytes, macrophytes, spores of non-vascular cryptogams and human-related pollen taxa as well as taxa with less than 1% of the total pollen sum, which is a threshold to differentiate between local pollen occurrences and long-distance transport. To avoid data bias and circularity, *Olea* was also removed from all pollen samples. The occurrences of the assigned modern species to the fossil pollen grains were crossed with modern climatology from the WorldClim database[64] to infer the climatic range of each fossil taxon. The values of the reconstructed climate variables (monthly mean, minimum and maximum temperature and monthly mean precipitation) correspond to the weighted median of the medians of the climatic ranges of all pollen taxa identified in each fossil sample, using pollen percentages as weights. The pollen-based model uncertainty is estimated by leaving one taxon out at each iterative reconstruction, with as many iterations as the number of taxa in each fossil sample. Reconstructions are provided with their estimated errors (chronological interpolation: 20-yr; Fig. 1), and with their long-term trends based on a polynomial model. All statistics and database analyses were performed using R software version 3.6.3[58] with Akima[65], RMySQL[66] and Stats libraries[58].

Present-day climate references for olive trees. Archived geographic occurrences of *O. europaea* (including several cultivars) in our database were cross-referenced with modern climatology from the CRU[67,68] to estimate monthly temperature and precipitation values for the species. This dataset, consisting of 325 stations (Extended Data Fig. 4), was used to estimate the present-day climatic range of *O. europaea* in the Mediterranean Basin. The temperature and precipitation are shown as the mean, the confidence interval (95%), and the 25th and 75th percentiles.

Climate projection. The 2100 temperature for each region, expressed as an anomaly from the 1961-1990 benchmark, was calculated based on the average rising rate between 1960 and 2020 (with the standard deviation). The average rising rate was then applied to the period 2021-2100. The 2100 temperature anomaly is indicated on each graph (Fig. 4). The raw data (1901-2020) are based on available long-term records[69].

Present-day olive oil. Lebanese olive-oil production (1991-2020) was obtained from the Lebanese Ministry of Economy[70] and the International Olive Council[26]. A Gradient species

packing was applied to define the optimum temperature and the tolerance zones (Extended Data Fig. 9a). The same test was applied to the Neolithic-Persian data. The optimum and tolerance zones were plotted against temperature (Extended Data Fig. 9b).

Data availability. All the raw data are available in the dataset (Figshare DOI: https://doi.org/10.6084/m9.figshare.21666830).

Acknowledgements

We wish to thank Dr Maha El-Khalil Chalabi (UNESCO Goodwill Ambassador, President of the Lebanese Committee of "Save Tyre") for her support in Lebanon. Financial support was provided by the MITI CNRS "Evénements rares", AQUASANMARCO program. Further support was provided by the ARKAIA Institute (Aix-Marseille University), the DRI (*École Pratique des Hautes Études*) and the *Partenariat Hubert Curien* (PHC) CEDRE. G.B. is supported by LabEx TULIP (ANR-10-LABX-0041) and the H2020 project Gen4Olive (H2020-SFS-2020-1; G.A. No. 101000427).

Author contributions

Conceptualization: DK, NM, RC, CM. Methodology: DK, NM, RC, CK, JFT, GB, TO, FL, QC, LT, MP, CM. Investigation: DK, NM, RC, CK, JFT, GB, TO, FL, QC, LT, MP, CM. Visualization: DK, NM, RC, CK, JFT, GB, TO, FL, QC, LT, MP, CM. Funding acquisition: DK, NM, CM. Supervision: DK, NM, RC, CM. Writing - original draft: DK, NM, RC. Writing - review & editing: DK, NM, RC, CK, JFT, GB, TO, FL, QC, LT, MP, CM.

Competing interests

The authors declare no competing interests.

Figures

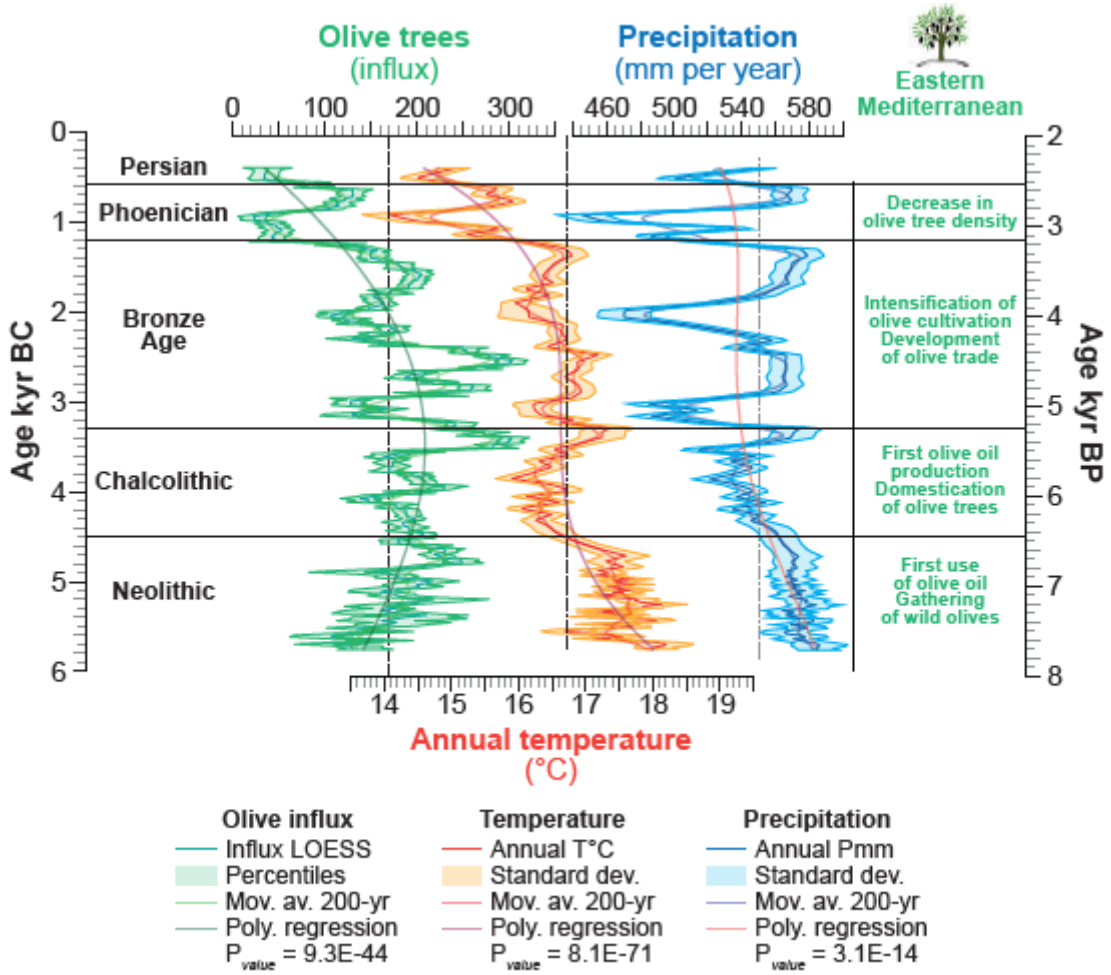

Figure 1. Olive influx compared with temperature and precipitation, from the Neolithic to the Persian period. The olive influx (*i.e.* number of pollen grains accumulated per unit of sediment surface and per unit of time; grains cm^{-2} yr^{-1}) is shown as a LOESS smoothing with the 2.5-97.5 percentiles (two-tailed). A 200-yr smoother and a polynomial regression (the P_{value} is based on a F test - two-tailed, with no adjustment) were added to describe the long-term trend. The annual temperatures (°C) and precipitation (mm) are shown with their standard deviations. Long-term trends were highlighted by polynomial regressions (the P_{value} is based on a F test - two-tailed, with no adjustment). The chronology is in kyr BP and BC. The main cultural periods are indicated on the graph. Eastern Mediterranean olive-tree facts are mentioned on the far-right column.

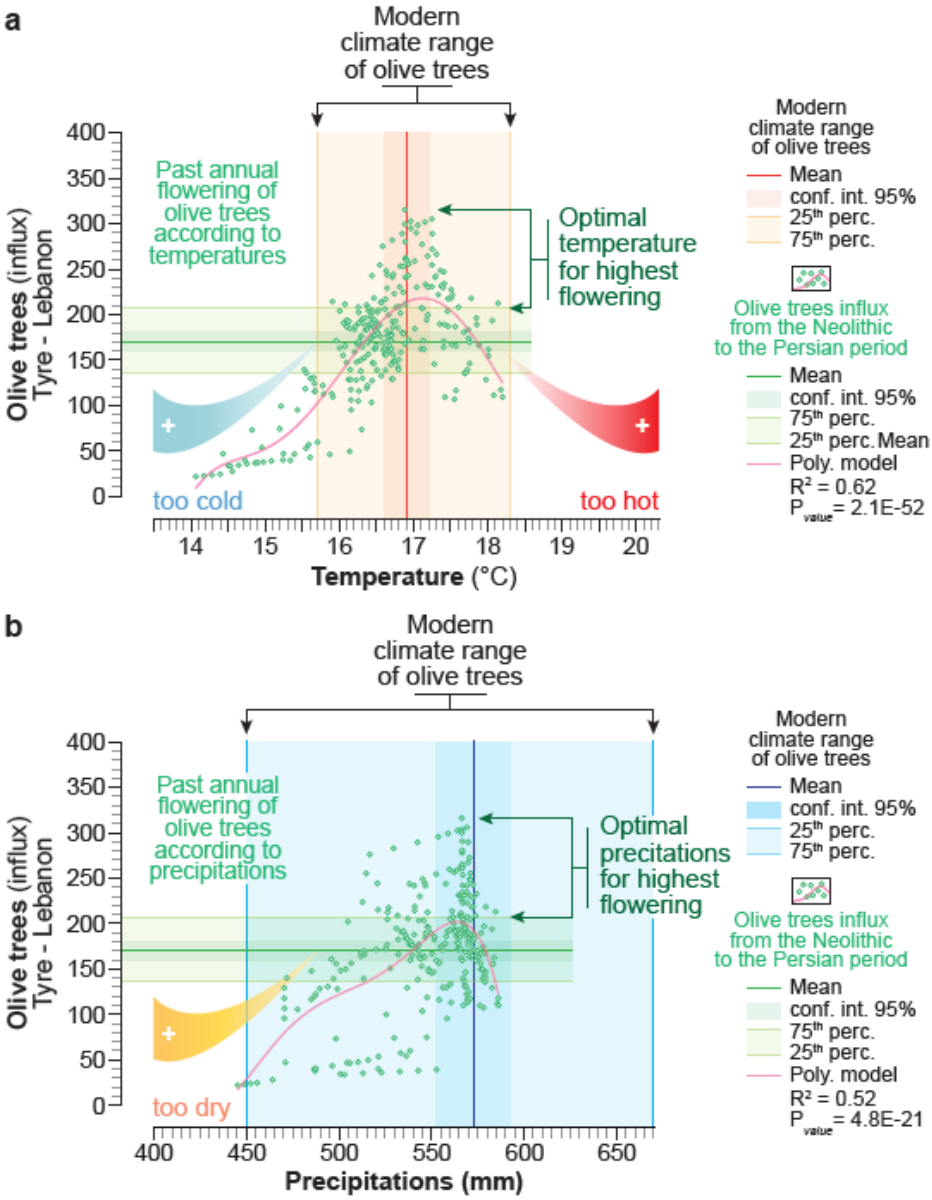

Figure 2. Distribution of olive influx according to temperature and precipitation. (**a**) Olive influx plotted against reconstructed annual T_{mean} (with the mean, 95% two-tailed confidence interval and 25th-75th percentiles). The long-term trend is highlighted by a polynomial regression (the P_{value} is based on a F test - two-tailed, with no adjustment). The data are contrasted with the present-day climate range of olive trees (optimum: average and 95% two-tailed confidence interval; full range: 25th and 75th percentiles). (**b**) Olive influx plotted against reconstructed annual precipitation (with the mean, 95% two-tailed confidence interval and 25th-75th percentiles). The long-term trend is highlighted by a polynomial regression (the P_{value} is based on a F test - two-tailed, with no adjustment). The data are contrasted with the present-day

climate range (optimum: average and 95% two-tailed confidence interval; full range: 25th and 75th percentiles).

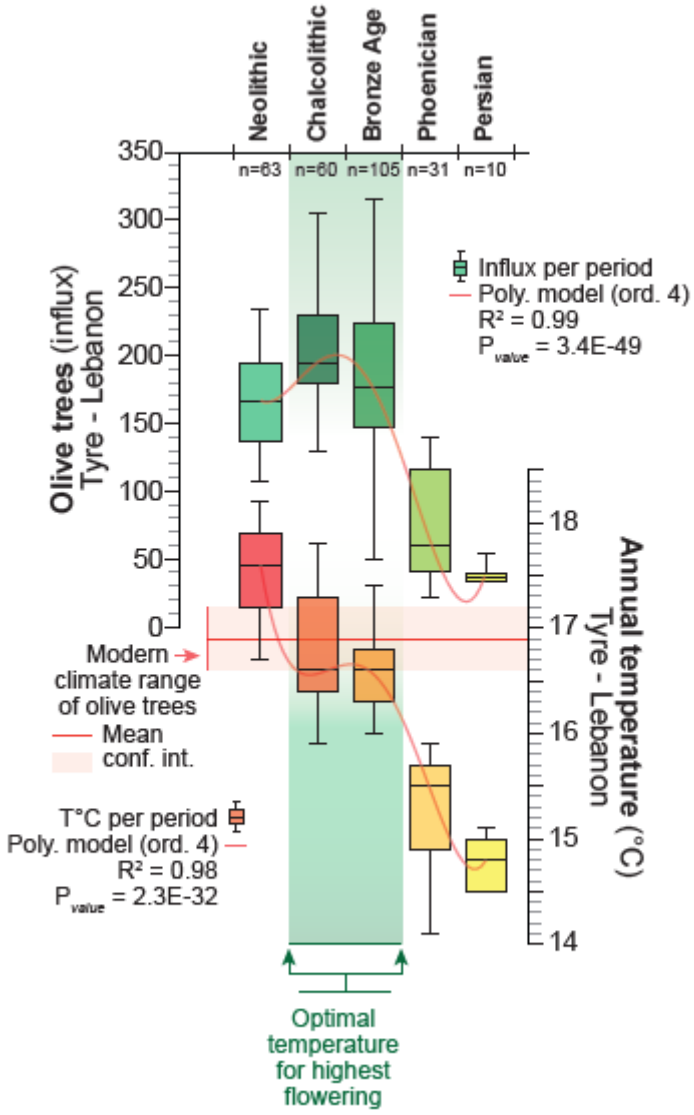

Figure 3. Pollen influx and temperature according to cultural periods. The pollen influx and reconstructed annual T_{mean} are shown as boxplots and organised by cultural periods. The boxplots depict the minima, maxima, the median values and the 25th-75th percentiles. The long-term trends are depicted by polynomial regressions (the P_{value} is based on a F test - two-tailed, with no adjustment). The present-day climate range of olive trees (optimum: average and 95% two-tailed confidence interval) is indicated on the graph.

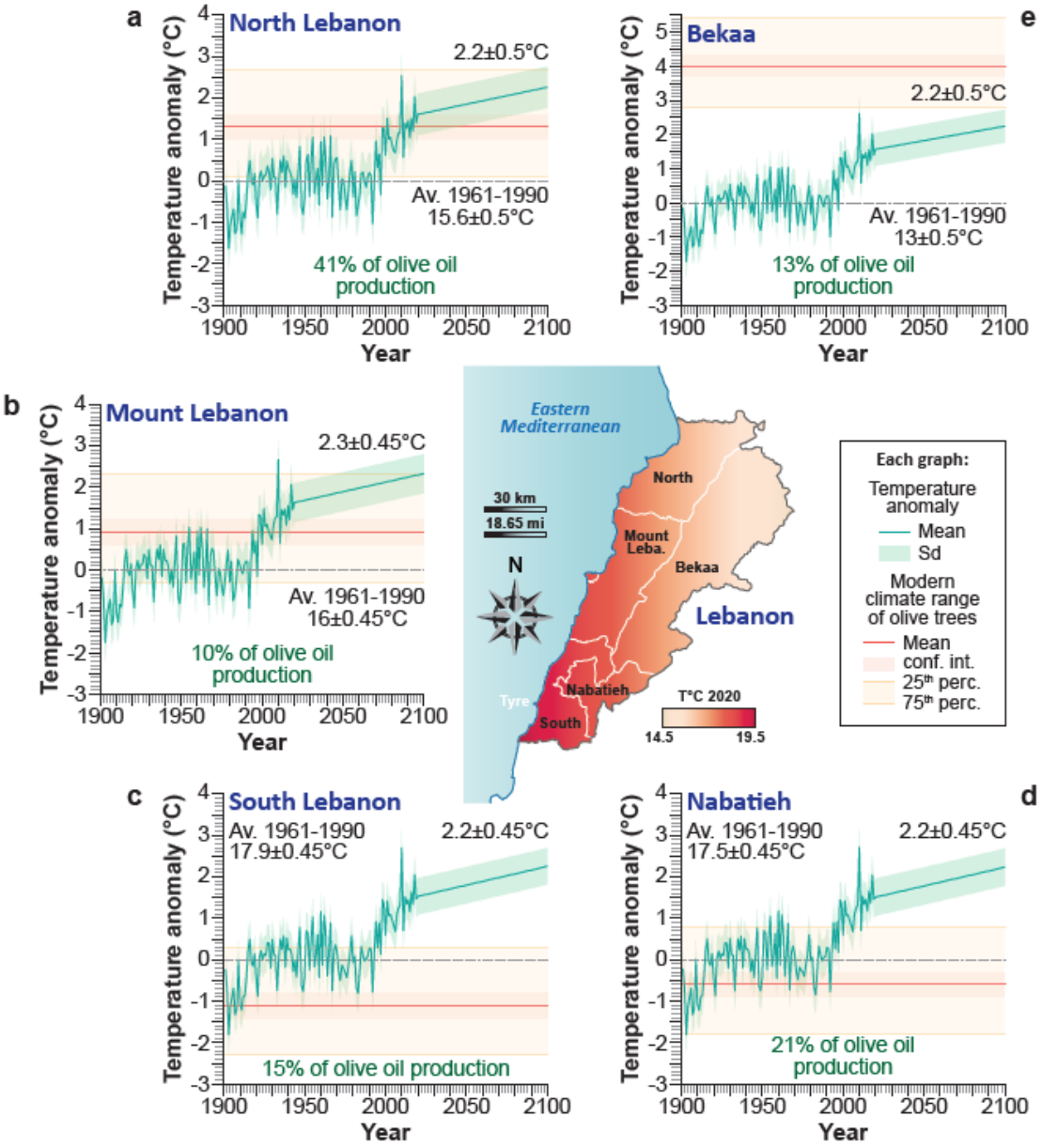

Figure 4. Climate projection per region for the year 2100 in Lebanon. The temperature is shown as an anomaly (mean and standard deviation) compared to the 1961-1990 baseline [by region with (**a**) North Lebanon, (**b**) Mount Lebanon, (**c**) South Lebanon, (**d**) Nabatieh and (**e**) Bekaa]. The projected temperature anomaly for the year 2100 is indicated on each panel. The present-day climate range of olive trees (optimum: average and 95% two-tailed confidence interval; full range: 25th and 75th percentiles) is denoted on each panel.

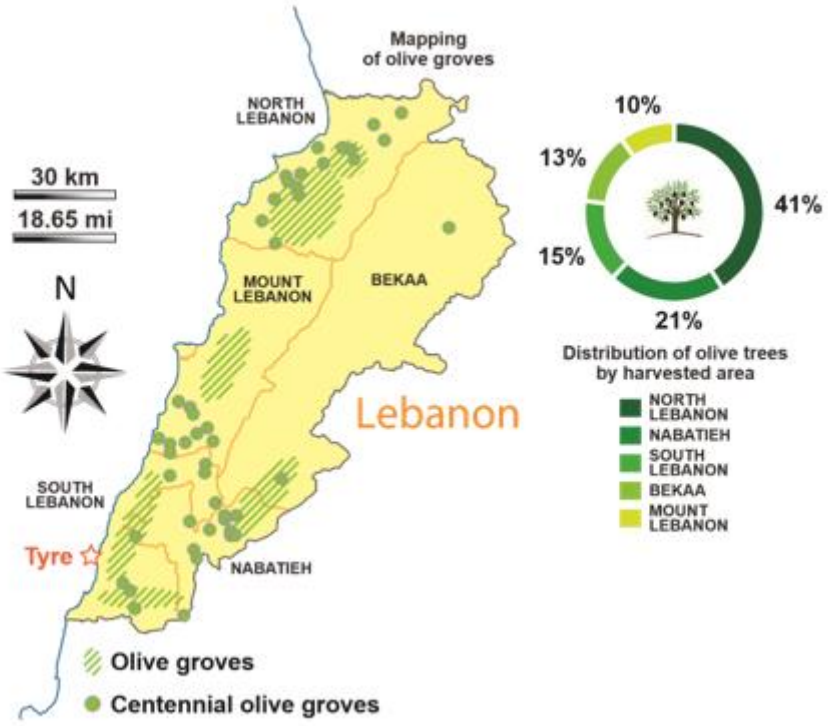

Extended Data Figure 1. Map showing centennial olive groves and the distribution of olive trees by harvested areas in Lebanon. The city of Tyre (South Lebanon) is indicated by an orange star. Data on olive groves derive from the literature[33]. The data on the distribution of olive trees by harvested areas derive from the Lebanese Ministry of Agriculture[31]. The map shows the five Lebanese regions used in this study.

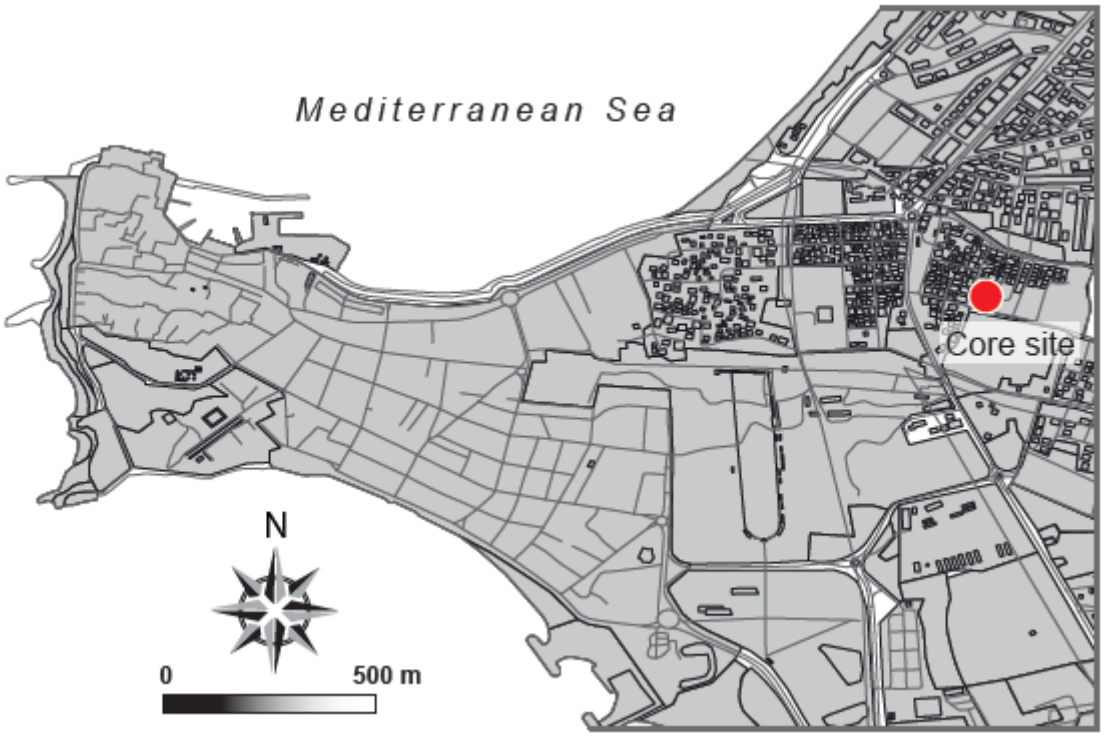

Extended Data Figure 2. Geographical location of the core T-XXI. The core was sampled near the Al-Bass necropolis, in the centre of Tyre.

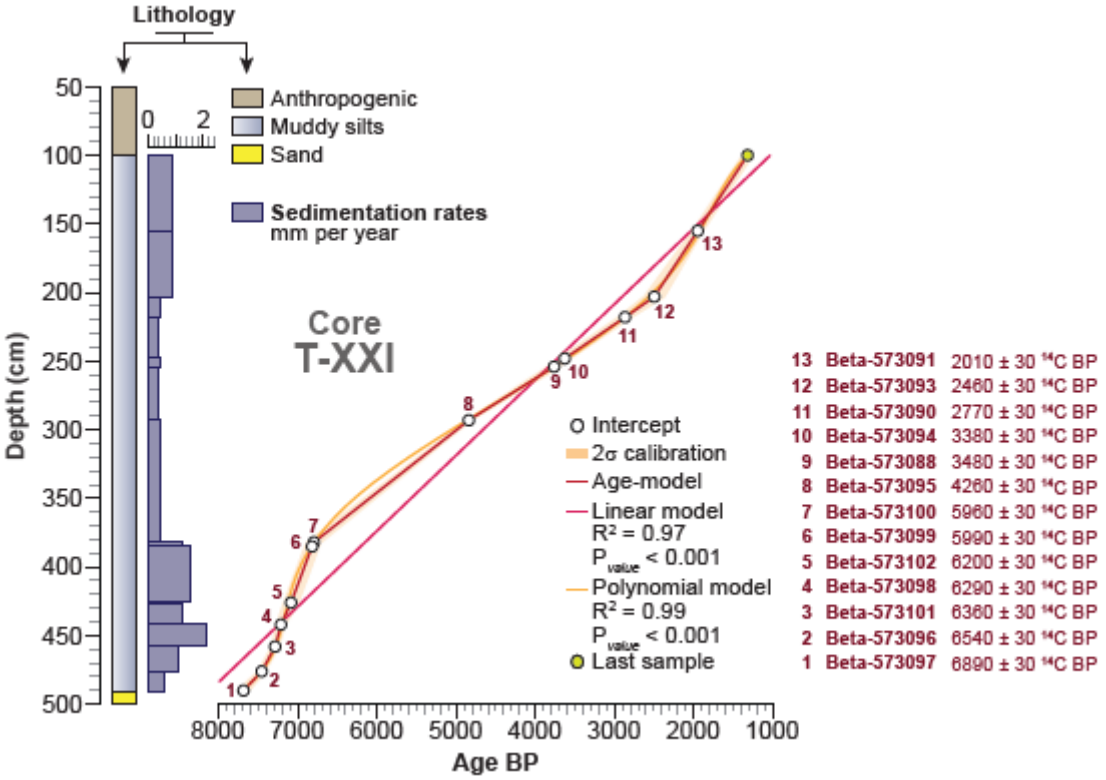

Extended Data Figure 3. Core T-XXI and the radiocarbon chronology. The lithology of the core is detailed according to depth (cm). The sedimentation rates are shown in mm per year. The radiocarbon dates are depicted as intercepts and 2-sigma calibrations (95% of probability, two-tailed). The age model (red curve) is compared and contrasted with linear (pink line; the P_{value} is based on a t test - two-tailed, with no adjustment) and polynomial (orange line; the P_{value} is based on a F test - two-tailed, with no adjustment) regressions. The radiocarbon dates, with their numbers, are detailed on the graph.

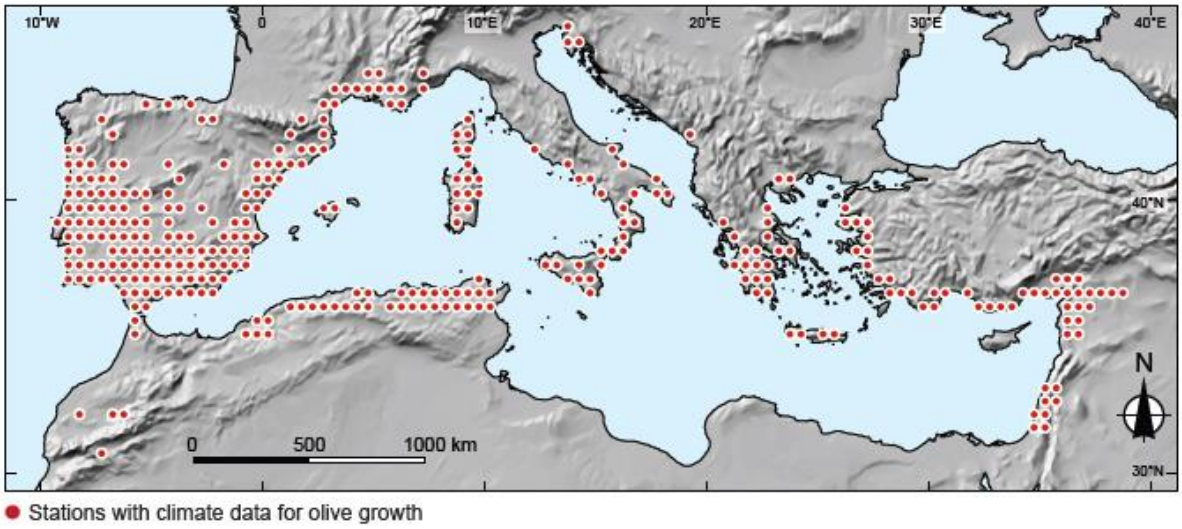

Extended Data Figure 4. Geographical location of the stations with climate data for olive growth. A total of 325 stations was used to estimate the present-day climatic range of *Olea europaea* in the Mediterranean Basin.

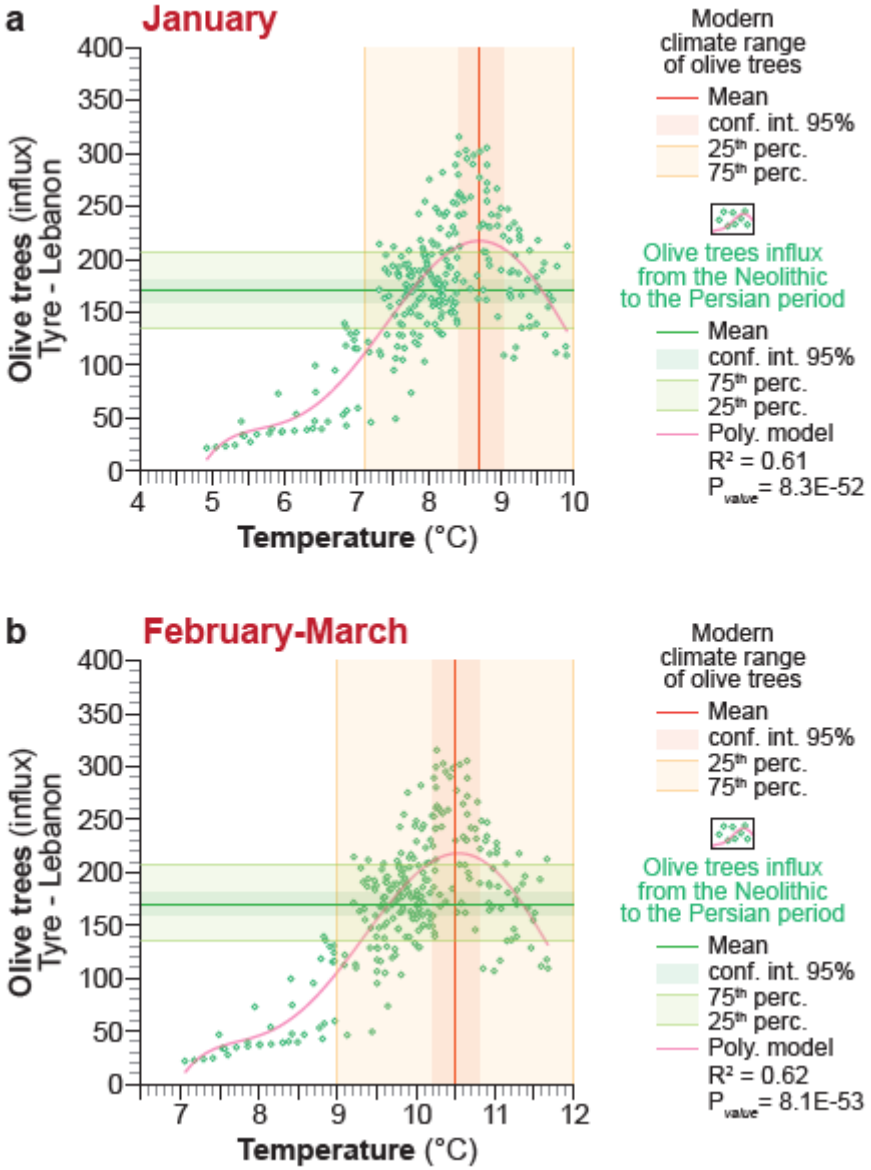

Extended Data Figure 5. Distribution of olive influx according to January and February-March temperatures. (**a**) Olive influx plotted against January temperatures (with mean, 95% two-tailed confidence interval and the 25th-75th percentiles indicated on the graph). The long-term trend is highlighted by a polynomial regression (the P_{value} is based on a F test - two-tailed, with no adjustment). The data are contrasted with the present-day climate range of olive trees in January (optimum: average and 95% two-tailed confidence interval; full range: 25th and 75th percentiles). (**b**) Olive influx plotted against February-March temperatures (with mean, 95% two-tailed confidence interval and the 25th-75th percentiles indicated on the graph). The long-term trend is highlighted by a polynomial regression (the P_{value} is based on a F test - two-tailed, with no adjustment). The data are contrasted with the present-day climate range of olive trees

in February-March (optimum: average and 95% two-tailed confidence interval; full range: 25th and 75th percentiles).

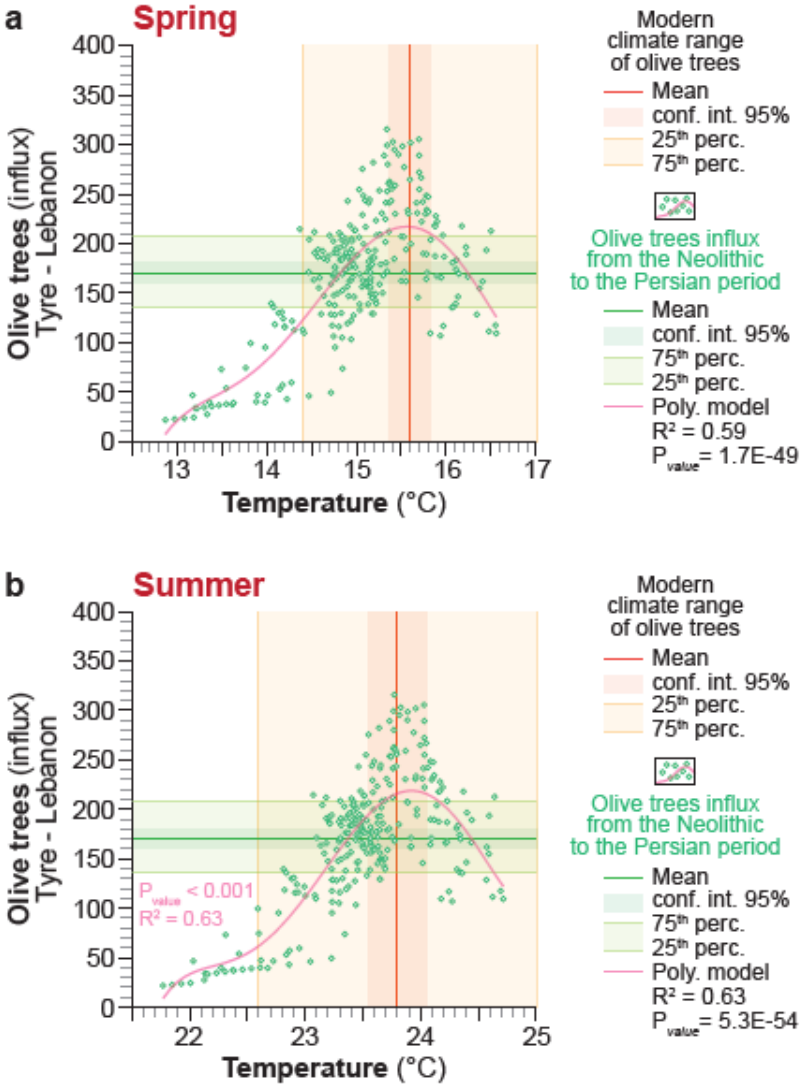

Extended Data Figure 6. Distribution of olive influx according to spring and summer temperatures. (**a**) Olive influx plotted against spring temperatures (with the mean, 95% two-tailed confidence interval and 25th-75th percentiles indicated on the graph). The long-term trend is highlighted by a polynomial regression (the P_{value} is based on a F test - two-tailed, with no adjustment). The data are contrasted with the present-day climate range of olive trees in spring (optimum: average and 95% two-tailed confidence interval; full range: 25th and 75th percentiles). (**b**) Olive influx plotted against summer temperatures (with the mean, 95% two-tailed confidence interval and 25th-75th percentiles indicated on the graph). The long-term trend

is highlighted by a polynomial regression (the P_{value} is based on a F test - two-tailed, with no adjustment). The data are contrasted with the present-day climate range of olive trees in summer (optimum: average and 95% two-tailed confidence interval; full range: 25th and 75th percentiles).

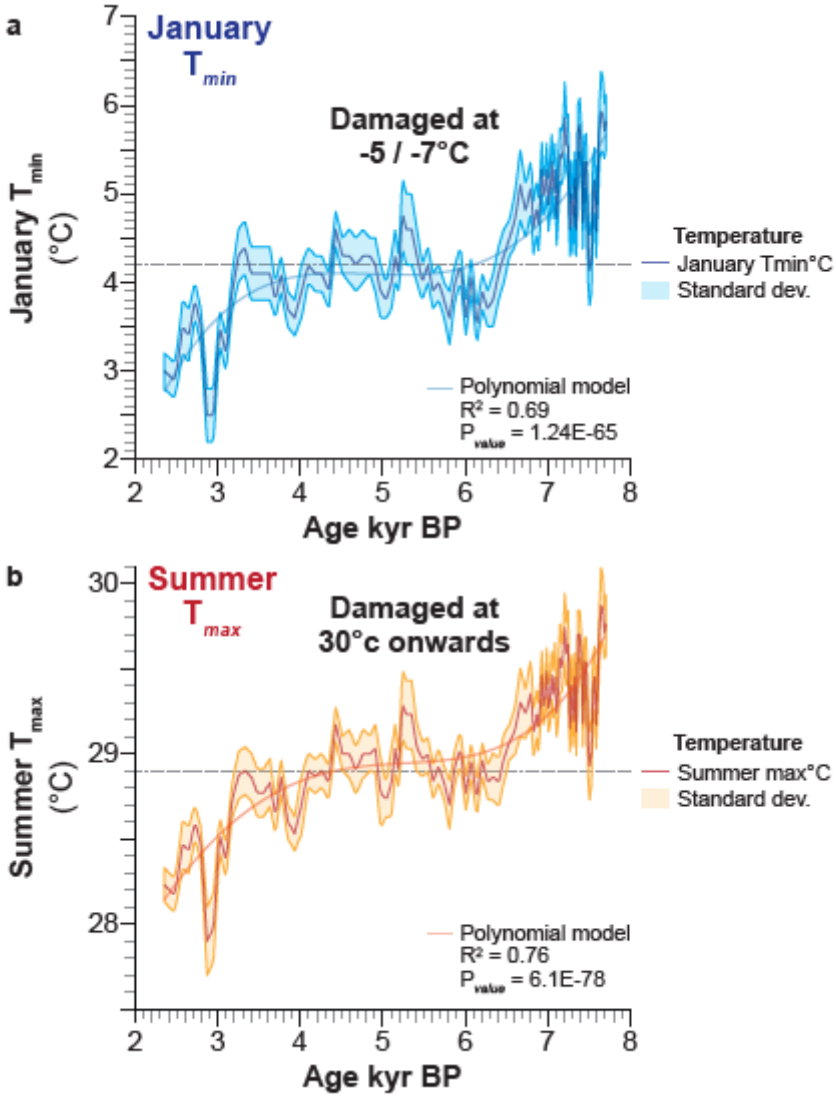

Extended Data Figure 7. Reconstructed T_{min} and T_{max} at Tyre from the Neolithic to the Persian period. (**a**) The T_{min} is shown for the colder period, January (mean and standard deviation). (**b**) The T_{max} is shown for the hotter period, Summer (mean and standard deviation). The temperature detrimental to olive-tree development is indicated on each panel.

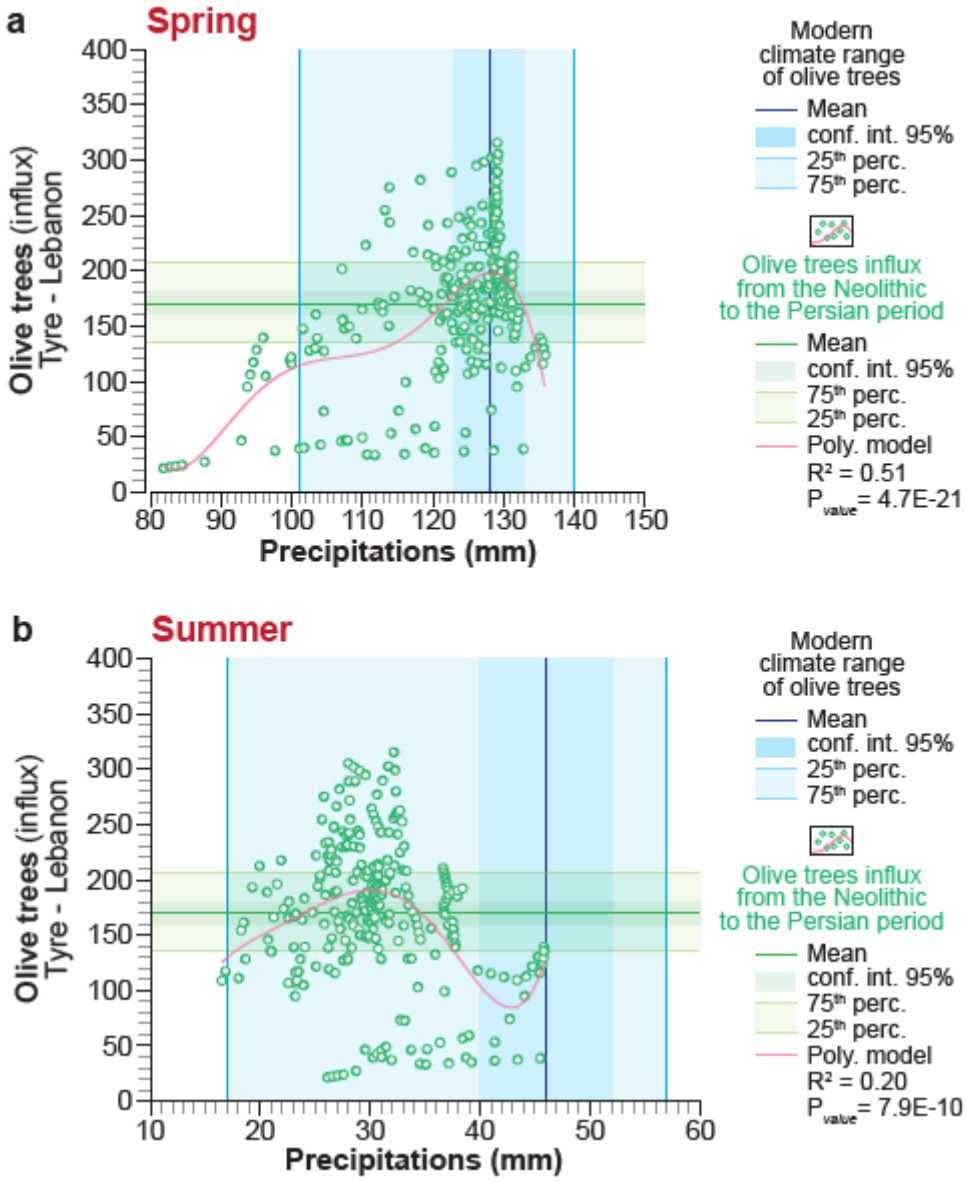

Extended Data Figure 8. Distribution of olive influx according to spring and summer precipitation. (**a**) Olive influx plotted against spring precipitation (with the mean, 95% two-tailed confidence interval and the 25th-75th percentiles). The long-term trend is highlighted by a polynomial regression (the P_{value} is based on a F test - two-tailed, with no adjustment). The data are contrasted with the present-day climate range of olive trees in spring (optimum: average and 95% two-tailed confidence interval; full range: 25th and 75th percentiles). (**b**) Olive influx plotted against summer precipitation (with the mean, 95% two-tailed confidence interval and the 25th-75th percentiles). The long-term trend is highlighted by a polynomial regression (the P_{value} is based on a F test - two-tailed, with no adjustment). The data are contrasted with the

present-day climate range of olive trees in summer (optimum: average and 95% two-tailed confidence interval; full range: 25th and 75th percentiles).

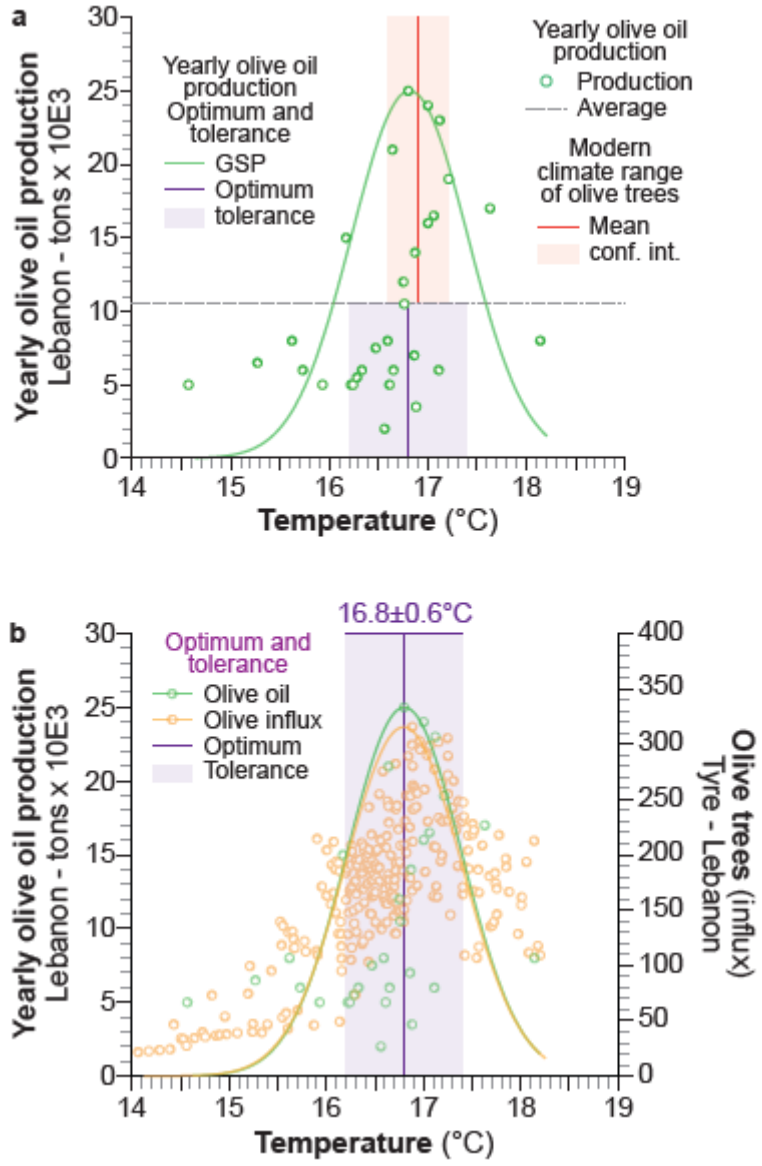

Extended Data Figure 9. Pollen influx compared with olive-oil production in Lebanon. (**a**) olive-oil production (period 1991-2020) is plotted against temperature recorded in northern Lebanon (main production region). The Gaussian curve (green curve) defined by the Gradient Species Packing (GSP) delineates an optimum and a tolerance zone for olive-oil production. The optimum and tolerance zones defined by the GSP are contrasted with the present-day climate range of olive trees (optimum: average and 95% two-tailed confidence interval). (**b**) Pollen influx and present-day olive-oil production plotted against temperature. The Gaussian

curves defined by the GSP show an optimum and a tolerance zone for olive influx (orange curve) and olive-oil production (green curve).

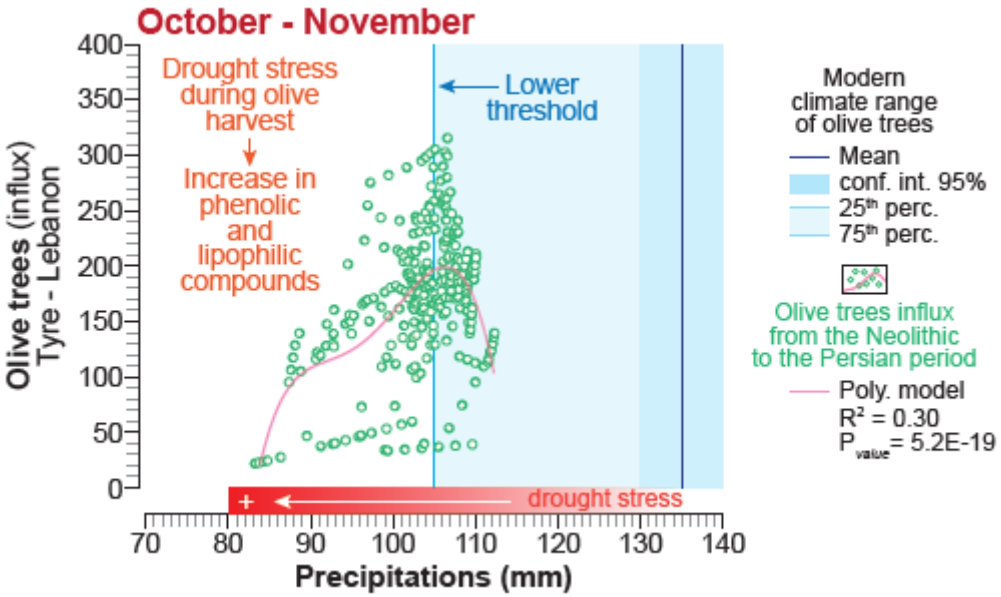

Extended Data Figure 10. Drought stress during the ripening and harvesting stages. Olive influx plotted against October-November precipitation. The long-term trend is highlighted by a polynomial regression (the P_{value} is based on a F test - two-tailed, with no adjustment). The data are contrasted with the present-day climate range of olive trees in October-November (optimum: average and 95% two-tailed confidence interval; with the 25th percentile).

References

1. Liphschitz, N., Gophna, R., Hartman, M. & Biger, G. The beginning of olive (*Olea europaea*) cultivation in the Old World: a reassessment. *J. Archaeol. Sci.* **18**, 441-453 (1991).

2. Blondel, J. & Aronson, J. *Biology and wildlife of the Mediterranean region* (Oxford University Press, 1999).

3. Fall, P. L., Falconer, S. E. & Lines, L. Agricultural intensification and the secondary products revolution along the Jordan Rift. *Hum. Ecol.* **30**, 445-482 (2002).

4. Terral, J.-F. et al. Historical biogeography of olive domestication (*Olea europaea* L.) as revealed by geometrical morphometry applied to biological and archaeological material. *J. Biogeogr.* **31**, 63-77 (2004).

5. Chartzoulakis, K. Salinity and olive: growth, salt tolerance, photosynthesis and yield. *Agric. Water Manag.* **78**, 108-121 (2005).

6. Vossen, P. Olive oil: history, production, and characteristics of the world's classic oils. *HortScience* **42**, 1093-1100 (2007).

7. Kaniewski, D. et al. Primary domestication and early uses of the emblematic olive tree: palaeobotanical, historical and molecular evidence from the Middle East. *Biol. Rev.* **87**, 885-899 (2012).

8. Langgut, D. et al. The origin and spread of olive cultivation in the Mediterranean Basin: The fossil pollen evidence. *Holocene* **29**, 902-922 (2019).

9. IPCC. AR5 Synthesis Report: Climate Change 2014. Switzerland, Geneva. https://www.ipcc.ch/report/ar5/syr/ (2014).

10. IPCC. IPCC WGII Sixth Assessment Report. Cross-Chapter Paper 4: Mediterranean Region. https://www.ipcc.ch/report/sixth-assessment-report-working-group-ii/ (2022).

11. Fischer, E. M. & Schär, C. Consistent geographical patterns of changes in high-impact European heatwaves. *Nat. Geosci.* **3**, 398-403 (2010).

12. Cramer, W. et al. Climate change and interconnected risks to sustainable development in the Mediterranean. *Nat. Clim. Change* **8**, 972-980 (2018).

13. Santos, J. A., Costa, R. & Fraga, H. Climate change impacts on thermal growing conditions of main fruit species in Portugal. *Clim. Change* **140**, 273-286 (2017).

14. Orlandi, F. et al. Impact of climate change on olive crop production in Italy. *Atmosphere* **11**, 595 (2020).

15. Rodríguez Sousa, A. A., Barandica, J. M., Aguilera, P. A. & Rescia, A. J. Examining potential environmental consequences of climate change and other driving forces on the sustainability of Spanish olive groves under a socio-ecological approach. *Agriculture* **10**, 509 (2020).

16. Besnard, G. et al. The complex history of the olive tree: from Late Quaternary diversification of Mediterranean lineages to primary domestication in the northern Levant. *Proc R Soc B* **280**, 20122833 (2013).

17. Besnard, G., Terral, J. F. & Cornille, A. On the origins and domestication of the olive: a review and perspectives. *Ann. Bot.* **121**, 385-403 (2018).

18. Bartolini, G., Prevost, G., Messeri, C., Carignani, C. & Menini, U. G. *Olive germplasm: cultivars and world-wide collections* (FAO-Rome, 1998).

19. Zohary, D. & Spiegel-Roy, P. Beginnings of fruit growing in the Old World. *Science* **187**, 319-327 (1975).

20. Terral, J.-F. Wild and cultivated olive (*Olea europaea* L.): a new approach to an old problem using inorganic analyses of modern wood and archaeological charcoal. *Rev. Palaeobot. Palynol.* **91**, 383-397 (1996).

21. Carrión, Y., Ntinou, M. & Badal, E. *Olea europaea* L. in the North Mediterranean basin during the Pleniglacial and the early-middle Holocene. *Quat. Sci. Rev.* **29**, 952-968 (2010).

22. Zohary, M. *Plants of the Bible* (Cambridge University Press, 1982).

23. Galili, E., Weinstein-Evron, M. & Zohary, D. Appearance of olives in submerged Neolithic sites along the Carmel Coast. *J. Israel Plant Sci.* **22**, 95-97 (1989).

24. Galili, E., Stanley, D. J., Sharvit, J. & Weinstein-Evron, M. Evidence for earliest olive-oil production in submerged settlements off the Carmel coast, Israel. *J. Archaeol. Sci.* **24**, 1141-1150 (1997).

25. Galili, E. et al. Early production of table olives at a mid-7th millennium BP submerged site off the Carmel coast (Israel). *Sci Rep* **11**, 2218 (2021).

26. International Olive Council. Available at: https://www.internationaloliveoil.org/ (2022).

27. Fraga, H., Pinto, J. G., Viola, F. & Santos J. A. Climate change projections for olive yields in the Mediterranean Basin. *Int. J. Climatol.* **40**, 769-781 (2020).

28. Ben Zaied, Y. & Zouabi, O. Impacts of climate change on Tunisian olive oil output. *Clim. Change* **139**, 535-549 (2016).

29. Brito, C., Dinis, L. T., Moutinho-Pereire, J. & Correia, C. M. Drought stress effects and olive tree acclimation under a changing climate. *Plants* **8**, 232 (2019).

30. Fraga, H., Moriondo, M., Leolini, L. & Santos J. A. Mediterranean olive orchards under climate change: a review of future impacts and adaptation strategies. *Agronomy* **11**, 56 (2021).

31. Ministry of Agriculture, Lebanon. Available at: http://www.agriculture.gov.lb/ (2022)

32. Trærup, S. & Stephan, J. Technologies for adaptation to climate change. Examples from the agricultural and water sectors in Lebanon. *Clim. Change* **131**, 435-449 (2015).

33. Chalak, L. et al. Extent of the genetic diversity in Lebanese olive (*Olea europaea* L.) trees: a mixture of an ancient germplasm with recently introduced varieties. *Genet. Resour. Crop. Evol.* **62**, 621-633 (2015).

34. Bou-Zeid, E. & El-Fadel, M. Climate change and water resources in Lebanon and the Middle. East. *J. Water Resour. Plan. Manag.* **128**, 343-355 (2002).

35. Ramadan, H. H., Beighley, R. E. & Ramamurthy, A. S. Sensitivity analysis of climate change impact on the hydrology of the Litani Basin in Lebanon. *Int. J. Environ. Pollut.* **52**, 65-81 (2013).

36. Saade, J., Atieh, M., Ghanimeh, S. & Golmohammadi, G. Modeling impact of climate change on surface water availability using SWAT model in a semi-arid basin: case of El Kalb River, Lebanon. *Hydrology* **8**, 134 (2021).

37. Halwani, J. & Halwani, B. in *Climate change in the Mediterranean and Middle Eastern region. Climate change management* (Eds. Leal Filho, W. & Manolas, E.) 395-412 (Springer, 2022).

38. Aubet, M.E. in *Nomads of the Mediterranean: trade and contact in the Bronze and Iron Ages* (Eds. Gilboa, A. & Yasur-Landau, A.) 14-30 (Brill, 2020).

39. Bikai, P. M. *The pottery of Tyre* (Aris & Phillips, 1979).

40. Hajar, L., Khater, C. & Cheddadi, R. Vegetation changes during the late Pleistocene and Holocene in Lebanon: a pollen record from the Bekaa Valley. *Holocene* **18**, 1089-1099 (2008).

41. Hajar, L., Haïdar-Boustani, M., Khater, C. & Cheddadi, R. Environmental changes in Lebanon during the Holocene: man vs. climate impacts. *J. Arid Environ.* **74**, 746-755 (2010).

42. Cheddadi, R. & Khater, C. Climate change since the last glacial period in Lebanon and the persistence of Mediterranean species. *Quat. Sci. Rev.* **150**, 146-157 (2016).

43. Ozturk, M. et al. An overview of olive cultivation in Turkey: botanical features, eco-physiology and phytochemical aspects. *Agronomy* **11**, 295 (2021).

44. Lionello, P., Congedi, L., Reale, M., Scarascia, L. & Tanzarella, A. Sensitivity of typical Mediterranean crops to past and future evolution of seasonal temperature and precipitation in Apulia. *Reg. Environ. Change* **14**, 2025-2038 (2014).

45. Arenas-Castro, S., Gonçalves, J. F., Moreno, M. & Villar, R. Projected climate changes are expected to decrease the suitability and production of olive varieties in southern Spain. *Sci. Total Environ.* **709**, 136161 (2020).

46. Mechri, B., Tekaya, M., Hammami, M. & Chehab, H. Effects of drought stress on phenolic accumulation in greenhouse-grown olive trees (*Olea europaea*). *Biochem. Syst. Ecol.* **92**, 104112 (2020).

47. Pedan, V., Popp, M., Rohn, S., Nyfeler, M. & Bongartz, A. Characterization of phenolic compounds and their contribution to sensory properties of olive oil. *Molecules* **24**, 2041 (2019).

48. Dias, M. C., Pinto, D. C. G. A., Figueiredo, C., Santos, C. & Silva, A. M. S. Phenolic and lipophilic metabolite adjustments in *Olea europaea* (olive) trees during drought stress and recovery. *Phytochemistry* **185**, 112695 (2021).

49. Peres, F. et al. Phenolic compounds of 'Galega Vulgar' and 'Cobrançosa' olive oils along early ripening stages. *Food Chem.* **211**, 51-58 (2016).

50. Tsimidou, M. Z. in *Handbook of olive oil: analysis and properties* (Eds. Aparicio, R. & Harwood, J.) 311-333 (Springer, 2013).

51. Valente, S. et al. Modulation of phenolic and lipophilic compounds of olive fruits in response to combined drought and heat. *Food Chem.* **329**, 127191 (2020).

52. WCRP. World Research Climate Program. Available at: https://www.wcrp-climate.org/wgcm-cmip/wgcm-cmip6 (2022).

53. Rallo, L. et al. in *Advances in plant breeding strategies: fruits* (Eds. Al-Khayri, J., Jain, S. & Johnson, D.) (Springer, 2018).

54. Abou-Saaid, O. et al. Statistical approach to assess chill and heat requirements of olive tree based on flowering date and temperatures data: towards selection of adapted cultivars to global warming. *Agronomy* **12**, 2975 (2022).

55. Faegri, K. & Iversen, I. *Textbook of pollen analysis, Fourth ed.* (Wiley, 1989).

56. Ferrara, G., Camposeo, S., Palasciano, M. & Godini, A. Production of total and stainable pollen grains in *Olea europaea* L. *Grana* **46**, 85-90 (2007).

57. Kaniewski, D. et al. Wild or cultivated *Olea europaea* L. in the eastern Mediterranean during the middle-late Holocene? A pollen-numerical approach. *Holocene* **19**, 1039-1047 (2009).

58. R Core Team. R: a language and environment for statistical computing. R Foundation for statistical computing, Vienna, Austria. Available at: https://www.R-project.org/ (2020).

59. Hammer, O. & Harper, D. *Paleontological data analysis* (Blackwell, 2006).

60. Cheddadi, R. et al. Microrefugia, climate change, and conservation of *Cedrus atlantica* in the Rif Mountains, Morocco. *Front. Ecol. Evol.* **5**, 114 (2017).

61. Kaniewski, D. et al. Cold and dry outbreaks in the eastern Mediterranean 3200 years ago. *Geology* **47**, 933-937 (2019).

62. Kaniewski, D. et al. Recent anthropogenic climate change exceeds the rate and magnitude of natural Holocene variability on the Balearic Islands. *Anthropocene* **32**, 100268 (2020).

63. Kaniewski, D. et al. Coastal submersions in the north-eastern Adriatic during the last 5200 years. *Global Planet. Change* **204**, 103570 (2021).

64. Hijmans, R. J., Cameron, S. E., Parra, J. L., Jones, P. G. & Jarvis, A. Very high-resolution interpolated climate surfaces for global land areas. *Int. J. Climatol. J. Royal Meteorol. Soc.* **25**, 1965-1978 (2005).

65. Akima, H. & Gebhardt, A. Akima: Interpolation of irregularly and regularly spaced data (Version 0.6-2, R package, 2016).

66. Ooms, J. D., Debroy, S., Wickham, H. & Horner, J. RMySQL: Database interface and 'MySQL' driver for R (Version 0.10.18, R package, 2019).

67. Climatic Research Unit. Available at: http://www.cru.uea.ac.uk/ (2022).

68. Harris, I., Jones, P. D., Osborn, T. J. & Lister, D. H. Updated high resolution grids of monthly climatic observations - the CRU TS3.10 Dataset. *Int. J. Climatol.* **34**, 623-642 (2014).

69. CCKP. Climate Change Knowledge Portal. Lebanon - Climatology. Available at https://climateknowledgeportal.worldbank.org/ (2022).

70. Ministry of Economy, Lebanon. Available at: https://www.economy.gov.lb/en (2022)